

NATURE OF RINGING ARTIFACTS IN SPECT RECONSTRUCTION AND THEIR REDUCTION BY THE USE OF SIDE INFORMATION

Jia Li

Dept. of Electrical and Computer Engineering
Oakland University
Rochester, MI 48309

Kenneth F. Koral

Department of Radiology
University of Michigan Medical Center
Ann Arbor, MI 48109-0552

ABSTRACT

ML-EM iterative reconstruction algorithms tend towards ringing artifacts, and high noise, after a large number of iterations just as filtered backprojection algorithms tend toward streak artifacts. OS-EM is a type of ML-EM algorithm and an edge overshoot has been observed experimentally for uniform-activity spheres of large size but not smaller size. Herein, we shed light on such artifacts by showing that they are a function of the object size relative to the FWHM of the collimator-detector response function. That is, for a given number of iterations, an over- or undershoot can occur at a given spatial location or not depending on the value of the ratio. We further show that a new, regularized, penalized-likelihood algorithm based on ordered subsets and employing side information stabilizes the iterative procedure against the development of artifacts.

1. INTRODUCTION

Single photon emission computed tomography (SPECT) is commonly used to obtain functional information for internal organs and tumors in nuclear medicine. A SPECT imaging system has a gamma camera rotating around the object to acquire projections at multiple angles. The SPECT image is usually reconstructed from the projections through filtered back projection or iterative reconstruction algorithm. The accuracy of quantitative applications of SPECT has been limited by the distortions in the reconstructed SPECT image. There are several known sources that can introduce distortions into SPECT. For example, Compton scattering and photoelectric absorption can be regarded as physical factors that cause errors in the SPECT projection data, the geometry of the collimators and the non-uniform sensitivity of the gamma camera are measurement factors that cause distortion in data acquisition, and the reconstruction algorithms, such as maximum likelihood-expectation maximization (ML-EM) and ordered subset expectation maximization (OS-EM) can cause high noise and edge artifacts [1].

In this paper, we discuss the image distortion caused by the ML-EM and OS-EM reconstruction algorithms, and how these distortions can be corrected by a regularized convergent ordered-subset (C-OS-3) algorithm. In Section 2, we describe different artifactual forms caused by the reconstruction algorithms and show that the edge artifacts and the underestimation or overestimation in the object center vary with the size of the object relative to the full width half maximum (FWHM) of the point spread function (psf). In Section 3, we discuss the C-OS-3 algorithm and propose to apply side information as a regularization in C-OS-3 to correct the image distortions mentioned in Section 2. We present simulation results comparing C-OS-3 to OS-EM in Section 4 and draw conclusions in Section 5.

2. RINGING ARTIFACTS

It has been observed that the SPECT images reconstructed by expectation-maximization algorithms, such as ML-EM and OS-EM, are more noisy and have strong edge artifacts when the total number of iterations in the reconstruction is large [1, 2].

2.1. Experimental Demonstration of Overshoot

An experimental demonstration of the overshoot artifact comes from SPECT acquisitions for a cylindrical phantom with an elliptical cross section that contained seven spheres [3]. The volumes of the spheres ranged from 209 to 4.2cc; they were well separated from each other and arranged at the center and six points of a hexagon as viewed from the top of the phantom. The largest sphere was placed at one depth in the cylinder, while the other six spheres were placed in another common depth. Each sphere was filled with water containing I-131 activity in approximately the same concentration, 43kBq/cc. The cylinder was filled with water containing I-131 activity in the concentration of 8.64kBq/cc. Thus, the activity concentration in the cylinder was in the proportion of 1 to 5 to the activity concentration in the spheres.

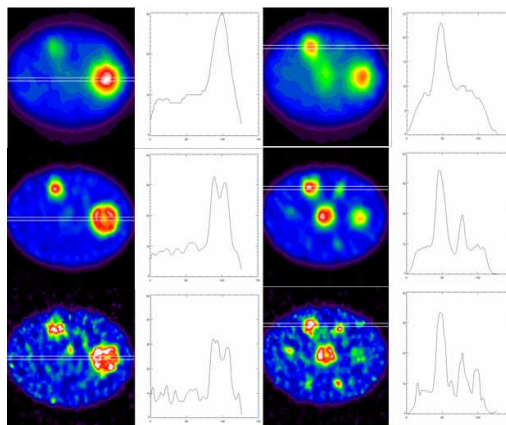


Fig. 1. Demonstration of dependence of artifact character on object size in OS-EM reconstructions of experimental data.

A Siemens Symbia SPECT/CT hybrid imager acquired 128x128 projection images of the phantom. Sixty angles over 360 degrees and a standard high-energy parallel-hole collimator were employed. Dynamic SPECT was used to obtain 10 sequential acquisitions of 15mins duration each. A CT image was acquired just before the

dynamic-SPECT series. Reconstruction was carried out with the Siemens software. The OS-EM algorithm used a constant-value initial guess. The psf for I-131 imaged with a high-energy collimator consists of a complex hexagonal-hole-pattern distribution for the main part of the response plus a six-ray septal-penetration star pattern. The Siemens depth-dependent model consisted of a rotationally-symmetric Gaussian with a full width half maximum that was slightly larger than that needed for the central part of the psf. The extra width accounted for the magnitude of the counts in the star pattern, although not for their spatial distribution. The CT image was automatically superimposed on the SPECT space. Attenuation correction was based on energy extrapolation of the CT values according to a Siemens prescription. The scatter corrupting the photopeak-window counts was estimated using the triple-energy-window method [4]. The estimates were employed during the OS-EM reconstruction. No post-reconstruction smoothing was applied to the images.

The 10 projection data sets were reconstructed with 8, 80, and 480 equivalent iterations, EI. Here EI is defined as the number of subsets times the number of iterations. For a given EI, the sum of all 10 reconstructions gives the surest indication of image artifacts, since statistical noise effects cancel out. These sum images are shown in Fig. 1. At the left is the slice and profile through the center of the 209cc sphere. At right, the slice and profile through the center of the 62.8cc sphere. From top to bottom, EI increases from 8 through 80 to 480. It is seen that the image for the large sphere develops an edge overshoot by EI=80. The image gets noisier, but the overshoot persists at EI=480. The image for the smaller sphere gets sharper, and then noisier, as EI increases. The sphere's profile does not display an edge overshoot. However, if one establishes the true counts/voxel for the 62.8cc sphere by a calibration based on the total counts within the geometric volume of interest for the 209cc sphere, then the counts/voxel in the central peak of the 62.8cc sphere profile is an overshoot after both 80 and 480 equivalent iterations.

2.2. Artifacts and the Ratio of Object Size over FWHM

Researchers believe that ringing artifacts occur because the reconstruction problem is ill-posed [1]. The experimental results shown above indicate that the type of artifact objects of the same shape develop is related to the object size. Fessler has conjectured that the form of distortion in the reconstructed image is related to the size of the object relative to the FWHM of the point spread function. He has supported that conjecture by carrying out ML-EM sharpening that simulated the ML-EM reconstruction of a 1D object [5]. That is, he used a 1D signal that was blurred by a psf. He then applied the version of ML-EM used in image restoration. This version is very similar to that employed in SPECT reconstruction. The system model is simply blur rather than blur and tomography. Below we reproduce the 1D result with his permission and in what follows we discuss it as if it were reconstruction.

In the 1D experiment, 70 rect functions, each having a different width, were used to represent the true activity distributions. The ML-EM algorithm reconstructed all the 1D functions. The FWHM of the psf was fixed at 12.02 pixels as shown in the lower left panel of Fig. 2. It has negatives because a subtraction was used to generate it. The images of truth, the projection data and the reconstructions are shown in the upper level from left to right. The width of the rects vary from 1 to 70 pixels. Edge artifacts are obvious for all the rect functions whose widths are larger than the FWHM. A profile is shown for the one with width = 49.7 at the middle bottom of the figure. The correct value is 3. The strength of the center and maximum

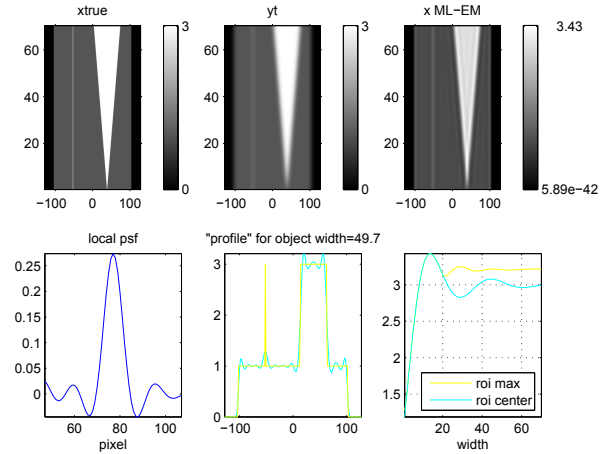


Fig. 2. Simulation of 1D reconstruction using ML-EM.

pixel are shown in the plots at the lower right. The edge overshoot is sometimes accompanied by an underestimation at the center location. For the rect functions with width less than the FWHM, the two overshooting peaks at the edge merge into one peak located at the center yielding the overestimation at the center location.

We have carried out a 2D reconstruction of noise-free simulated data to provide a more direct verification of the Fessler conjecture. Three uniform-activity disks, each of a different size, are used as the objects. The disk diameters are 10, 6 and 4 pixels. In simulating the projection data, the size of all the disks was fixed. However, the FWHM of the psf was increased from one simulation to the next, and then the psf with the appropriate FWHM value was used in each OS-EM reconstruction. The number of iterations employed in each reconstruction was 200.

The results are shown in Fig. 3. Fig. 3(a) shows the true image, while Fig. 3(b) and (c) show the reconstructed images and the profiles passing through the center of the object for different FWHM. It can be seen from the profile that the total number of rings in the large disk is greater than the total number of rings in the smaller disks when FWHM is small. For example, when FWHM equals 2 pixels, the number of peaks in the large, middle and small disks are 4, 3 and 2, respectively. For all three disks, the total number of rings decreases as the value of FWHM increases until the ring effect is completely replaced by an overshoot effect in the center of the disks. However, the overshoot effect begins occurring at a different FWHM depending on the size of the disk. For example, the center overshoot begins at FWHM=3 for the small disk, at FWHM = 5, for the mid-size disk, and at FWHM = 8 for the large disk. This verifies the conjecture that the form of distortion caused by an EM-type algorithm is correlated with the size of the object relative to the FWHM of the psf. A linear regression between the size of object and the FWHM value of the psf at which the center overshoot begins occurring is shown in Fig. 4. The strong linear correlation verifies the conjecture that for a given number of reconstruction iterations, the artifacts can occur at a given spatial location or not depending on the ratio of object size to the FWHM of the psf.

3. REGULARIZATION THROUGH SIDE INFORMATION

Some techniques have been proposed to correct the image distortions shown in Section 2. In [1], Snyder et al proposed using a blurring

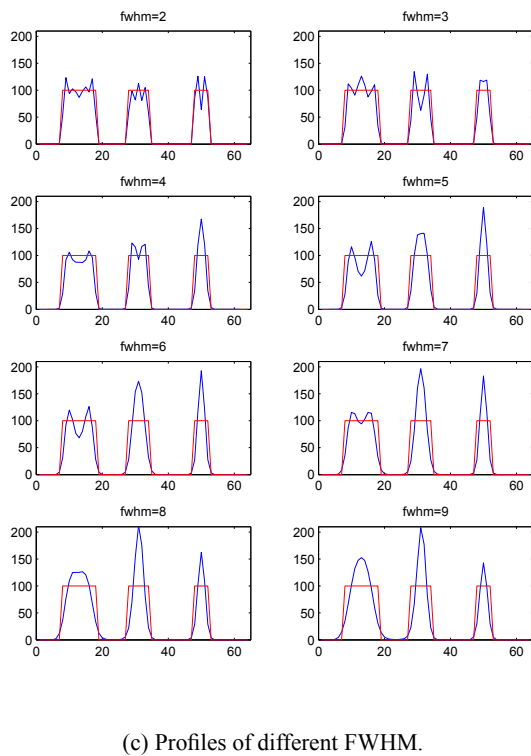
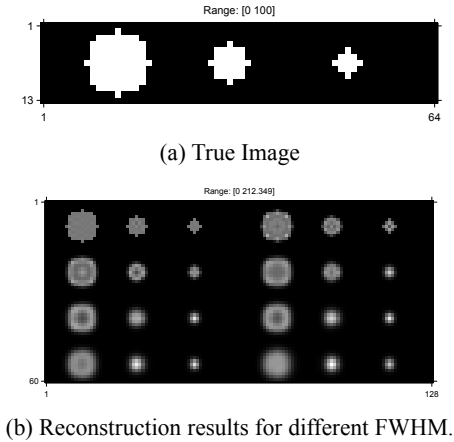


Fig. 3. Reconstruction of simulated 2D projection data using 200 iterations of OS-EM.

kernel in the EM algorithm to suppress the edge artifacts. However, the use of blurring function can reduce the resolution of the reconstructed image, which may cause inaccuracy in quantitative applications, such as tumor dose estimation. The ideal approach is to impose different regularizations in the target region and the background region so that sharp boundaries can be preserved and different types of noise and distortions can be addressed by different constraints. This requires proper side information to distinguish the different regions.

Before the emergence of hybrid SPECT/CT systems, side information was usually utilized through image fusion of SPECT and CT from different imaging sessions, where the accuracy of the side in-

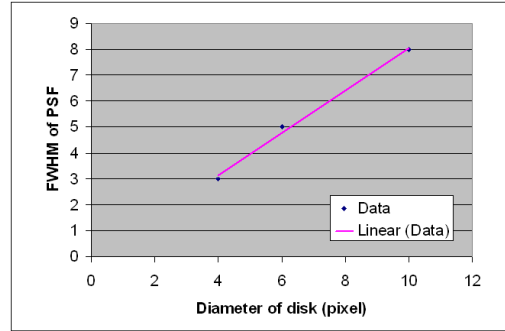


Fig. 4. The correlation between object size and the FWHM value of the psf in the case where center overshoot begins occurring.

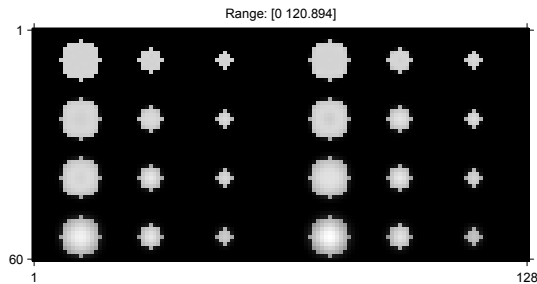
formation was limited by the adopted fusion procedure. In a hybrid SPECT/CT system, the CT scanner and the gamma camera are integrated in one imaging system with a patient translated between the two imagers. This allows automatic and accurate fusion of the two types of data sets provided the patient doesn't move, although the fusion is still subject to the degradation caused by respiration. CT data have long been used to generate attenuation maps for SPECT reconstruction. Other than the attenuation map, side information has also been used in edge-preserving SPECT reconstructions and SPECT-CT fusions.

To eliminate the artifacts shown in Section 2, we propose using side information in the convergent ordered-subsets 3 (C-OS-3) algorithm to get a penalized-likelihood SPECT reconstruction. The C-OS-3 algorithm belongs to the framework of convergent incremental optimization transfer methods described in [6]. Specifically, it is an extension of the convergent C-OSEM algorithm of [7] that is based on an incremental version of the complete-data space used in the EM-3 algorithm described in [8]. The algorithm is available in Matlab code in the Image Reconstruction Toolbox written by Fessler [5]. Unlike OS-EM or typical regularized versions thereof, C-OS-3 does converge to the penalized-likelihood estimate. That estimate is unique because the convex regularizer used in the work ensures that the cost function is strictly convex. C-OS-3 converges a bit faster than C-OSEM in the presence of an additive scatter term. In the hypothetical case where scatter / room background is zero, C-OS-3 and C-OSEM are identical algorithms [6].

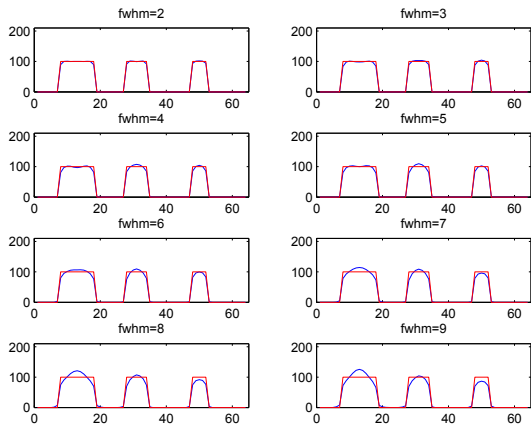
4. REGULARIZATION RESULTS

We have carried out noise-free simulations to demonstrate that the regularized C-OS-3 algorithm employing side information can efficiently reduce ringing artifacts. The simulated projections of the three objects that yielded the results in Section 2 are used again, but are this time reconstructed by C-OS-3. We assume that perfect side information is available from a hybrid SPECT/CT system. The side information consists of knowing the location of the edge of each of the three disks and providing it to the C-OS-3 algorithm. The collimator-detector-response model used to generate the projection data and that used in the reconstructions are depth-independent Gaussians. The eight sets of projection data corresponding to the eight different values of FWHM were reconstructed.

Fig. 5 shows the reconstruction results. Fig. 5(a) is the reconstructed image, while Fig. 5(b) is the profile passing through the center of the objects. If we compare the results in Fig. 5 with the results in Fig. 3, we see that the ringing artifacts have been almost



(a) Reconstructed image.



(b) Profile passing through the object center.

Fig. 5. Reconstruction results for regularized C-OS-3 algorithm employing side information after 200 iterations.

completely removed in the cases with FWHM between 2 to 5. We notice that in the cases of FWHM between 6 to 9, there is overshoot in the center of the large object, and underestimation near its edge. We also notice that the total activity in the reconstructed small object decreases as the value of FWHM increases. We think this phenomenon occurs due to the low pass filtering effect caused by the large value of FWHM. That is, the large FWHM causes activity to spill outside the object. Apparently, it cannot be recovered even with the penalty based on the side information.

Table 1 compares the total activity recovered within appropriate geometrical ROIs for the three objects using the two different algorithms. The recovered activity is expressed as a percentages of the true activity. The FWHM of the Gaussian model equals 4 pixels. It can be seen that the C-OS-3 algorithm regularized by side information gives better activity recovery as compared to the traditional OS-EM algorithm, assuming one wants to stop after a reasonably-small number of iterations (200). A convergence plot for total counts shows that if you are willing to iterate 2,000 times, you can improve the OSEM activity recovery considerably, although not much for the middle disk. If you are willing to iterate 10,000 times, you get good recovery with OS-EM for all disk sizes in this case. However, the ringing artifacts remain.

Reconstruction Method	Left Disk	Middle Disk	Right Disk
OSEM	96.3	91.2	88.8
C-OS-3 with side information	98.1	98.1	98.3

Table 1. Comparison of total activity recovered for the case with FWHM = 4 pixels.

5. CONCLUSIONS

In this paper, we showed that the ringing artifacts in SPECT images reconstructed by the OS-EM algorithm are related to the FWHM of the collimator-detector-response model. We propose using a new, regularized C-OS-3 algorithm employing side information to eliminate the artifacts. The simulation results show that the proposed algorithm can greatly reduce the ringing effects as well as improve the total activity recovered within a geometrical ROI. In the future, we want to investigate how counting-statistics noise and the level of the background surrounding the object affect the artifacts' relationship to the FWHM of the psf.

6. ACKNOWLEDGMENTS

We want to thank Prof. Jeffrey Fessler at the University of Michigan for allowing us to use his image reconstruction toolbox and for many helpful discussion about this research.

7. REFERENCES

- [1] D. Snyder, M. Miller, L. Thomas, and D. Politte, "Noise and edge artifacts in maximum-likelihood reconstructions for emission tomography," *IEEE Trans. on Medical Imaging*, vol. 6, no. 3, pp. 228–238, 1987.
- [2] B. Tsui, E. Frey, X. Zhao, D. Lalush, R. Johnson, and W. McCarty, "The importance and implementation of accurate 3D compensation methods for quantitative SPECT," *Physics in Medicine and Biology*, vol. 39, no. 3, pp. 509–530, 1994.
- [3] K. Koral, J. Kritzman, V. Rogers, R. Ackermann, and J. Fessler, "Optimizing the number of equivalent iterations of 3D OSEM in SPECT reconstruction of I-131 focal activities," *Nuclear Instruments and Methods in Physics Research*, 2006, in press.
- [4] K. Ogawa, H. Harata, T. Ichihara, A. Kubo, and S. Hashimoto, "A practical method for position dependent compton-scatter correction in single photon emission CT," *IEEE Trans. on Medical Imaging*, vol. 10, pp. 408–412, 1991.
- [5] J. Fessler, "Image reconstruction toolbox," <http://www.eecs.umich.edu/~fessler>.
- [6] S. Ahn, J. Fessler, D. Blatt, and A. Hero, "Convergent incremental optimization transfer algorithms: Application to tomography," *IEEE Trans. on Medical Imaging*, vol. 25, no. 3, pp. 283–296, 2006.
- [7] I. Hsiao, A. Rangarajan, P. Khurd, and G. Gindi, "An accelerated convergent ordered subsets algorithm for emission tomography," *Physics in Medicine and Biology*, vol. 49, no. 11, pp. 2145–2156, 2004.
- [8] J. Fessler and A. Hero, "Penalized maximum-likelihood image reconstruction using space-alternating generalized EM algorithms," *IEEE Trans. on Image Processing*, vol. 4, no. 10, pp. 1417–1429, 1995.